Steady State Creep Characteristics of a Ferritic Steel at Elevated Temperature: An Experimental and Numerical Study

Roozbeh Alipour*
Department of Mechanical Engineering,
Mahshahr Branch, Islamic Azad University, Mahshahr, Iran
E-mail: r.alipour@mhr.ac.ir
*Corresponding author

Ali Farokhi Nejad
Dipartimento di ing. Meccanica e Aerospaziale,
Politecnico di Torino, Corso Duca degli Abruzzi, Torino, Italy
E-mail: ali.farokhi@polito.it

Hamid Nilsaz Dezfouli
Department of Industrial Engineering,
Mahshahr Branch, Islamic Azad University, Mahshahr, Iran
E-mail: h.nilsaz@mhriau.ac.ir

Abstract: Prediction of creep life for a ferritic steel plate is significant in the context of its application as an element of steam generating systems. In this paper, the issue of elevated temperature creep in 2.25Cr–1Mo steel was investigated in detail, including the mechanism and the compatibility of hyperbolic sine modeling methodology for the description of steady state creep behavior of this alloy. Creep rupture tests were conducted on the thin foil samples at an elevated temperature ranging from 973 to 1073 K at various stresses between 90 to 210 MPa. A hyperbolic sine model is then used to fit the experimental creep data and the corresponding best fit parameters are provided. Using these parameters, a finite element analysis employing ABAQUS was carried and the reliability of the hyperbolic sine model was investigated in relation to the creep curve and creep life in the steady state creep area. The main outcome of the current study is creep characterisation of 2.25Cr–1Mo steel foils at extreme elevated temperature and to propose a finite element model for simulating this condition which is not reported so far. The results of experimental, constitutive analysis and finite element simulation were compared to each other and it was shown that they are in a good agreement.

Keywords: Creep, Finite Element Analysis, Ferritic Steel, Hyperbolic Sine Model

Biographical notes: Roozbeh Alipour received his PhD in Applied Mechanics and Mechanical Engineering from UTM, MY, 2016. He is currently Senior Lecturer at the Department of Mechanical Engineering, Mahshahr branch, Islamic Azad University, Mahshahr, Iran. **Ali Farokhi Nejad** is a PhD Scholar in the Department of Mechanical and Aerospace engineering at Politecnico di Torino, Italy. **Hamid Nilsaz** is Assistant Professor in the Department of Industrial Engineering, Mahshahr branch, Islamic Azad University, Mahshahr, Iran.

1   INTRODUCTION

Ferritic steels are typically iron-chromium alloys possessing BCC crystal structures that W, Mo, C, N, Nb and V, one or all, can be found in their combination as the alloying elements [1-4]. Among the ferritic alloys, 2.25Cr–1Mo steel is an operational structural material which is extensively used in steam generating equipment of power plants and petroleum or petrochemical industries. The components of these systems are commonly exposed to relatively elevated temperatures for a long while, experiencing time dependent creep deformation and damage. The mentioned consequences result from the formation, growth, and coalescence of cavities and also from the enhanced microstructural degradation in the form coarsening of precipitates and dislocation substructure under stress [5]. Hence, it is necessary to study the creep rupture life of these alloys in the presence of an excessive load and elevated temperature for robust design of components [6]. It leads to manage the creep phenomenon and increase the level of safety for such facilities which operate at elevated temperature.

For 2.25Cr–1Mo structural steel which is extensively used in the steam generating systems in all over the world, there are two serious challenges in incorporating creep behavior prediction at elevated temperature applications. First challenge is the lack of existing experimental creep data for this alloy and the second is the deficit of the investigation of available constitutive creep model to simulate the experimental data. The former challenge was recently addressed in a series of researches to some extent. For instance, the effect of triaxial stress state on creep lifetime of 2.25Cr–1Mo steel has been evaluated by Goyal et al. [7], wherein they conducted creep tests on circumferential and plain U-notch samples for various notch acuity ratios. In a similar study, the recent author and his co-workers [8] investigated the effect of the multi-axial state of stress on creep rupture behavior of 2.25Cr–1Mo steel. Results indicated that, the creep damage in this material under mentioned loading condition was predominantly in the form of microstructural degradation with some pieces of evidence of intergranular creep cavitation especially at lower stresses. There are other reports on the effect of stress relaxation loading cycles [9-10] and steamside oxidation and fireside corrosion degradation processes [11] on the creep behavior of 2.25Cr–1Mo. Residual life assessment method based on the quantitative analysis of change of precipitate free zone around grain boundaries during long-term creep was presented by Nguyen et al [12]. In a different experimental study, creep rupture tests were performed on 2.25Cr–1Mo steel to estimate the service life of the reactor internals made of this alloy [13]. The common point about these recent researches is to conduct the creep tests at maximum 650°C, while the

more elevated temperature has not been examined on this alloy thus far. To address the latter challenge, the creep models of power law kind of stress dependence [14] and Dyson–McLean [15] were employed to model the experimental creep behavior but no accurate fit could be observed. Also, these investigations were not concentrated on the creep of thin foil specimens which is mainly used in the turbochargers. Thus, the topic of appropriate creep model for the thin foil of 2.25Cr–1Mo alloy especially in the area of FE simulation can be still supposed open to discuss.

In this paper, the issue of elevated temperature creep in 2.25Cr–1Mo steel is investigated in detail, including the mechanism and the compatibility of hyperbolic sine modeling methodology for the description of steady state creep behavior of this alloy. To evaluate the creep behavior and life, creep rupture tests are conducted on the thin foil samples at an elevated temperature ranging from 973 to 1073 K at various stresses between 90 to 210 MPa. Next, the hyperbolic sine law for modeling of creep is examined, and it is investigated whether or not the mentioned model for 2.25Cr–1Mo steel is compatible to describe the creep behavior at elevated temperature and high stress states. This investigation not only characterizes the creep behavior of alloy in steady state step, but also helps to describe this behavior analytically. Based on the obtained model, a steady state FE analysis was carried out and the results were compared with the experiments. This latest step highlights the possibility of using hyperbolic sine model in FE simulation of creep behavior of 2.25Cr–1Mo especially in deal with complicated structural geometry.

1.1. Literature Review and Background of Study

While the creep phenomenon is closely in conjunction with microstructural variations during material deformation, a continuum description of the creep process can be of great engineering importance. As a result, several researches have been reported to amplify the reliable procedures for predicting the behavior of thin metal foils which operate subjected to the creep condition [16-18]. Various mathematical and numerical models supported by experimental verification have been developed in conjunction with predicting the creep behavior of metals [19]. Most of them are based on the results of individual uni-axial tension creep [20-21] in which, the creep phenomenon occurs in the following three steps [22]: In the primary step, the strain starts at a rapid rate, but slows with increasing time and most related to the work hardening. In the next step, known as secondary or steady-state creep, the strain rate eventually attains a minimum and becomes near constant value which is due to the balance between work hardening and thermal softening. This step is very significant since the term "creep strain rate" typically addresses the strain rate in this secondary step. The last step is called tertiary creep in which the strain rate

exponentially raises with stress as regards of necking phenomena or internal voiding reduces the effective area of the specimen and always end up with the fracture. The Norton [23], the Dyson–McLean [24], the Kachanov-Rabotnov [25], the Theta-Projection [26-27] and the Modified Theta-Projection [28-30] models are some examples of usual creep models which describe the creep phenomenon based on the mentioned triple steps. From the standpoint of the structural integrity design, the secondary step of creep is often most interesting for the engineers [31].

Therefore, several creep rate laws have been proposed by the researchers to cover this step and the majority of them including the Norton power law model [32] and the hyperbolic sine modeling methodology [33-34]. The hyperbolic sine law is able to describe the flow behavior of material subjected to elevated temperature, which contains wide stress and strain rate ranges. The importance of the hyperbolic sine modeling methodology becomes more highlighted considering the power law model and has been proven to be more useful for creep and superplastic flow at elevated temperatures and lower strain rates with low stresses [35]. Nevertheless, failure of the power law model at high stresses is well known since the stress exponent rises with stresses and varies with strain rates [36]. There are the other creep models such as the exponential law [37] which breaks down at elevated temperatures and strain rates blow 1s−1 [38]. So it may be appropriate to apply the hyperbolic sine law to specify the true stress exponent and activation energy during creep deformation of metals at elevated temperature combining with high stresses.

There are several reports on creep behavior characterization of some structural steels such as ASTM A992 [39], ASTM 709 [40], A36 [41] and etc. in the steady state step. Further advancements in the characterization of creep for operational structural material such as 2.25Cr–1Mo have been limited due to the lack of relevant experimental creep data and the corresponding constitutive models which were validated for such material. However, the significance of creep in elevated temperature applications has been attracted attentions by various researches [42-44]. In a study, Liao et al. [45] used the hyperbolic sine constitutive equation to model the flow stress of annealed AZ61 magnesium alloys subjected to the compression load at the temperatures ranging from 250°C to 450°C and at the strain rates ranging from 10−3 s−1 to 1 s−1. The flow stresses of these alloys were estimated well by the constitutive equations of the hyperbolic sine function under the loading conditions of the study. Cui et al. [46] examined the creep behavior of 316L(N) austenitic stainless steel subjected to various stresses and temperatures ranging from 525 °C to 700 °C. Results showed an acceleration of the creep deformation during the last 15% of creep lifetime, which contributes to macroscopic necking. Also, the modeling of necking using the Norton viscoplastic power-law was in good agreement with experimental data in the case of creep lifetime prediction.

Zhang et al. [47] employed finite element (FE) method to investigate the creep crack initiation position and incubation time of P92 steel pipes with embedded spherical defects at 650 °C. It was shown that the creep crack most often initiates on one side of a spherical defect, near either the outer surface or the inner surface of the pipe. To calculate the shifting time, the analytical formulations were proposed, while less attention was paid to computational models to estimate this parameter. Although many studies have been conducted on 2.25Cr–1Mo, but considering that the maximum operating temperature of the turbine supercharger is higher than 800 C˚, and with the increase in temperature, the creep rate increases, less attention has been paid to the creep behaviour of this material at extremely elevated temperatures, hence the significance of the present study becomes more important.

2   EXPERIMENTAL PROCEDURE

2.1. Material and Geometry of Specimens

The experimental material was a cold-rolled forming thin foil of 2.25Cr–1Mo alloy with an analyzed chemical composition as given in "Table 1", measured by induction-coupled plasma and spark optical emission spectrometry apparatuses. Due to the low thickness of foil, a wire-cut machine was used to cut the foil in the appropriate dimensions for preparing the specimens. Flat specimens with a height of 114 mm and a thickness of 0.2 mm were machined from the foil along the axial direction for the uni-axial tensile tests. The titanium pin-hold grips were used to ensure the uniaxial tension of the 0.2 mm-thin foil specimen and no moment applying to the foils. Figure 1 indicates the geometry and dimensions of the specimens.

Table 1. The chemical composition of the material

Element	C	Mn	Si	P	S	Cr	Mo	Fe
(wt %)	0.06	0.55	0.17	0.009	0.008	2.27	0.97	Bal
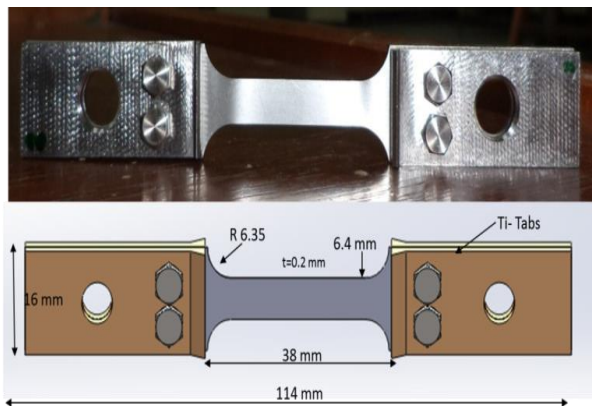
Fig. 1   Geometry and dimension of the creep test specimens.

2.2. Experiments

Elevated temperature phenomenological creep models for steel alloys are typically formulated by evaluating the creep data extracted from experiments. Creep tests were conducted based on ASTM E139 [48]. The experiments were carried out at temperatures $1023 \pm 2K$ and at different extreme stress levels of 90 to 210 MPa, under an air environment. Moreover, in order to obtain the standard deviation value for material characterization, the tests were repeated in 973 K and 1073 K at the applied stresses 110, 130, and 150 MPa. A dead-load knife-edge lever creep machine with three-zone furnace was used. Test temperature was controlled using a proportional-integral-derivative (PID) controller. Thermocouples were connected at both sides of gauge length of the specimen to monitor the temperature. Due to the thickness of foils and in order to avoid bending and torsion along the specimen, the blocker pins were used in the upper and lower side of creep machine. After applying the calculated load for each test, the blocker pin was removed slightly. Creep strains were measured in the uniaxial loading using a couple of linear variable differential transformers (LVDT). The LVDTs were attached to the lower side of extensometer. The data from extensometer, the load cell and the thermocouples are collected in a data logger for the data analysis in the characterization step. Figure 2 shows the setup of experiments before starting the tests. The morphology of creep failure for specimens was conducted using Field Emission Scanning Electron Microscopy (FESEM). The specimens for metallographic examination were etched with Klemm reagent.
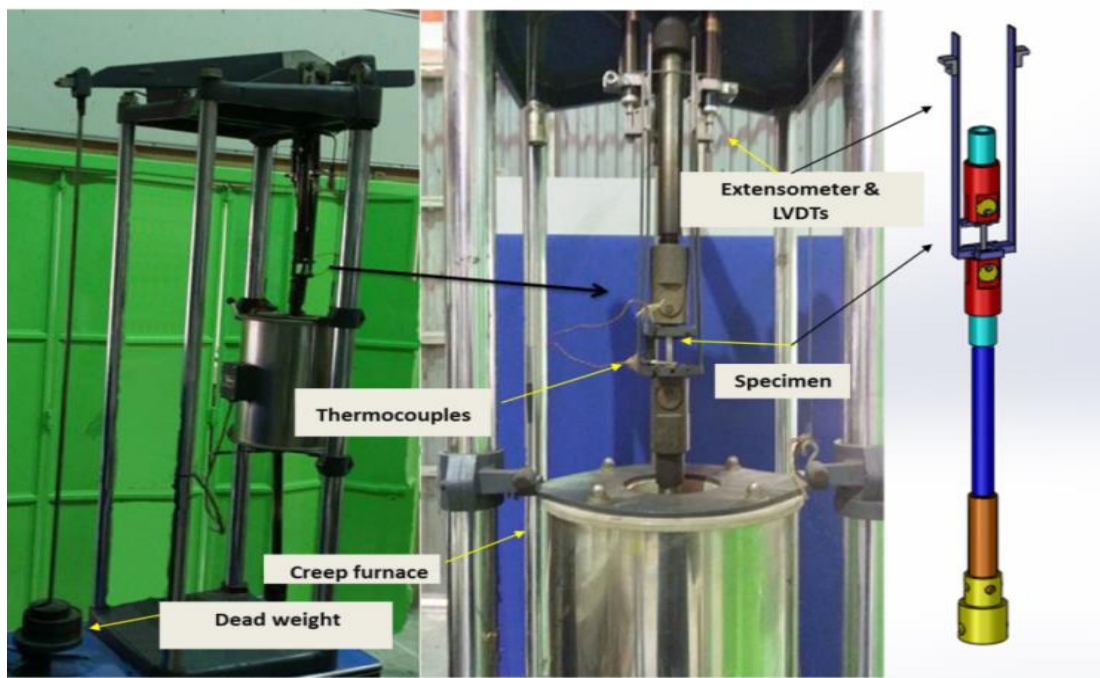
Fig. 2   Setup of the experiment for creep tests.

3   CREEP CONSTITUTIVE MODEL FOR 2.25CR–1MO ALLOY

It is realized from the previous sections that the creep models are phenomenological and formulated to fit the obtained experimental data. In this section a creep model for 2.25Cr–1Mo alloy is proposed that can be employed for modelling of steady state creep at elevated temperatures and high stresses state. To this end, the creep data for 2.25Cr–1Mo alloy extracted from section 2 is used. This creep data has a high level of significance

since 2.25Cr–1Mo alloy steel is widely used in the construction of power plant turbochargers, and the experimental creep data of thin foil for this alloy has been rarely reported.

As mentioned earlier, due to the weakness of power law and exponential law for modeling the creep behavior at different conditions, the hyperbolic sine modeling methodology is more employed to demonstrate the stress rate function at high stresses state and elevated temperature. In order to calculate the flow stress of metallic material at elevated temperature, the Arrhenius term is used [49-50]. In this case the, the creep strain rate is expressed as follows [45]:

$$\dot{\varepsilon}_{cr} = A\big[\sinh\ (\alpha\sigma)\big]^{n}\left[\frac{-Q}{RT}\right] \tag{1}$$

In which, A (s^{-1}) and α (MPa^{-1}) are constants, σ is the uniaxial equivalent deviatoric stress or flow stress (MPa), n is the stress exponent, R is the universal gas constant, T is the absolute temperature (K), and Q is the activation energy (kJ mol^{-1}). Considering the activation energy, the rate-controlling mechanism can be assessed. By rearranging "Eq. 1" and taking the natural logarithms of both sides, it can be rewritten as "Eq. 2".

$$\ln\ [\sinh\ (\alpha\sigma)] = \frac{1}{n}\ln\dot{\varepsilon}_{cr} + \frac{Q}{nR}\ (\frac{1}{T}) - \frac{1}{n}\ln A \tag{2}$$

Where α is an adjustable multiplier that sets $\alpha\sigma$ into a range in which, the lines in a diagram plotted by $\ln \dot{\varepsilon}_{cr}$ against $\ln\ [\sinh\ (\alpha s)]$ become parallel at a given temperature. Hence, the parallelism of these lines is checked using the standard deviation considering the average n [45]. Descriptions of the operation required to reach an appropriate α can be found in [51-52] in detail. Based on "Eq. 2", the slope of the line in the $\ln \dot{\varepsilon}_{cr} - \ln$ [$\sinh\ (\alpha s)$] plot at a given temperature and strain is defined by n. If the "Eq. 2" rearranged and differentiated with respect to $1/T$, the following expression is achieved that can be employed to determine the activation energy, Q, at a specified strain and strain rate:

$$Q = R\ \frac{\partial\ \ln\dot{\varepsilon}_{cr}}{\partial\ \ln[\sinh\ (\alpha\sigma)]}\ \big|_{\varepsilon,T}\ \frac{\partial\ \ln[\sinh\ (\alpha\sigma)]}{\partial\ (\sfrac{1}{T})}\ \big|_{\varepsilon,\dot{\varepsilon}} \tag{3}$$

Where the second term in the right side of "Eq. 3" expresses the average slope of the plotted lines between $\ln \dot{\varepsilon}_{cr}$ and $\ln\ [\sinh\ (\alpha s)]$ and the latest term refers to the average slope of the lines which are plotted $\ln\ [\sinh\ (\alpha s)]$ versus $1/T$. The creep strain rate can be related to the Zener-Hollomon parameter [53], Z, which is expressed as:

$$Z = \dot{\varepsilon}_{cr}\exp\left[\frac{Q}{RT}\right] \tag{4}$$

In this case, the "Eq. 1" is transformed to the Z form expression as follow:

$$Z = A\ [\sinh\ (\alpha\sigma)]^{n} \tag{5}$$

By applying the natural logarithm on both sides of "Eq. 5", it can be rewritten as:

$$\ln Z = \ln A + n\ln\ [\sinh\ (\alpha\sigma)] \tag{6}$$

By plotting the $\ln Z$ against $\ln\ [\sinh\ (\alpha\sigma)]$ considering Q and n obtained from "Eqs. 2 and 3", the material constant A is calculated. Thus, all the parameters of creep hyperbolic sine equation in elevated temperature for this ferritic steel foils can be characterized using this methodology.

4   FINITE ELEMENT ANALYSIS

In this study, the numerical simulations were conducted employing the nonlinear FE code ABAQUS 6.12. Model of the thin foil was developed using hexahedral elements with 8 nodes (C3D8R) based on the experimental specimen dimension and geometry. After convergence study, element sizes of 0.35mm for the specimen were chosen to achieve acceptable results. Similar boundary conditions to the experiment were applied to the model. In order to avoid stress concentration at the supporting region, the end sides of the specimen were fixed with the coupling technique.

An iterative implicit solver [54-56] considering the nonlinear geometry capability was used. The hyperbolic sine creep model available in ABAQUS material library was employed for the modeling the creep. The data for the creep hyperbolic sine model that was extracted from experiments (section 2) was used to describe the behavior of the specimen during the creep loading. Different loads were applied to simulate different stress level.

The temperature filed with 1023 K was induced along the specimen during the simulation. The analyses were conducted in two steps: first, the temperature was initialized and the stress was applied. Next, the specimen was allowed to creep at a constant stress and temperature. The difference in axial displacement across the gage length is used to measure the creep strains that developed. An FE model of a specimen is shown in "Fig. 3".
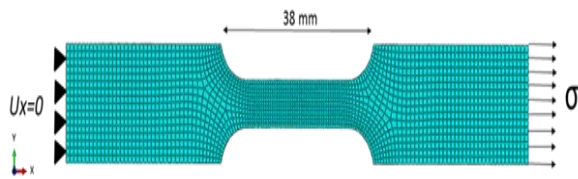
Fig. 3   An FE model of a specimen.

5   RESULTS AND DISCUSSION

5.1. Creep Behavior of 2.25Cr–1Mo Alloy under Axial State of Stress

Creep experiments were conducted on the 2.25Cr–1Mo alloy at 973, 1023 and 1073 K over a range of stress. The specimens at 1023 K were subjected to the 90, 110, 130,

150, 170, 190 and 210 MPa stresses. However, the specimens at 973 and 1023 K were undergone the 110, 130 and 150 MPa stresses just to ensure obtaining the same trend of creep behavior at 1023 K.

Figure 4 shows the variations of creep strain against time at different stresses. The creep deformation of 2.25Cr–1M alloy was characterized by a small instantaneous strain on loading, an apparent secondary stage, followed by a prolonged tertiary creep regime. The primary step of creep was removed from the experimental results for illustration on a logarithmic scale. A short transient and a prolonged tertiary stage illustrated that the strain hardening in the material rapidly recovered at such a high homologous temperature. It is obvious that, the rupture strains at different levels of loading are close to some extent, however the rupture time as the most critical parameter may attribute to the applied stress.
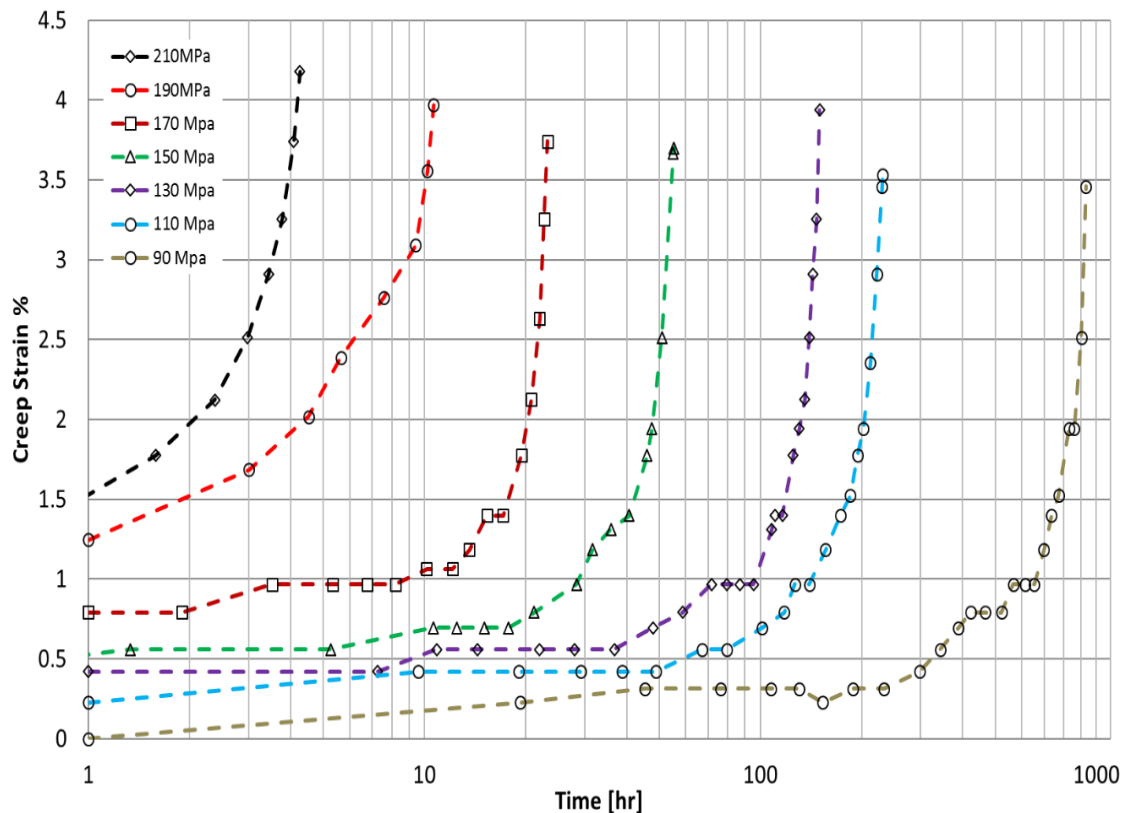
Fig. 4   Variation of creep strain with creep exposure of the 2.25Cr–1Mo steel at 1023 K for various stresses.

5.2. Creep Failure Mechanism

Figure 5 shows the typical microstructure of 2.25Cr-1Mo steel alloy after creep testing at 1027 K under 150 MPa. Morphology examination of creep-ruptured foil samples tested using optical and scanning electron microscope (FESEM) reveals trans-granular fracture characterized by dimples resulting from

coalescence of micro-voids at all applied stresses.

Extensive carbides precipitation, particularly in the grain, can be observed. It seems that these particles were composed of carbides such as M23C6, M6C and M2C at the grain boundaries. This is likely due to the thermally activated annihilation of voids and defects along the grain boundary and the simultaneous stretching of the

grains by a high localized tensile load. The creep cavitations of w-type were seen at the junction of grain boundaries more severe in "Fig. 5 (b)". These voids form at the triple-point grain boundaries where the self-diffusion rate is not high enough to relieve the stress concentrations. Under continuous creep straining, these voids can link up to separate the grain boundaries and

rapidly weaken the material leading to inter-granular fracture. At the elevated temperature, chromium atoms diffuse to the grain boundary and form carbide precipitates. During the test, the depletion of adjacent grain matrix in Cr causes sensitization of the alloy leading to loss of the resistance to corrosion.
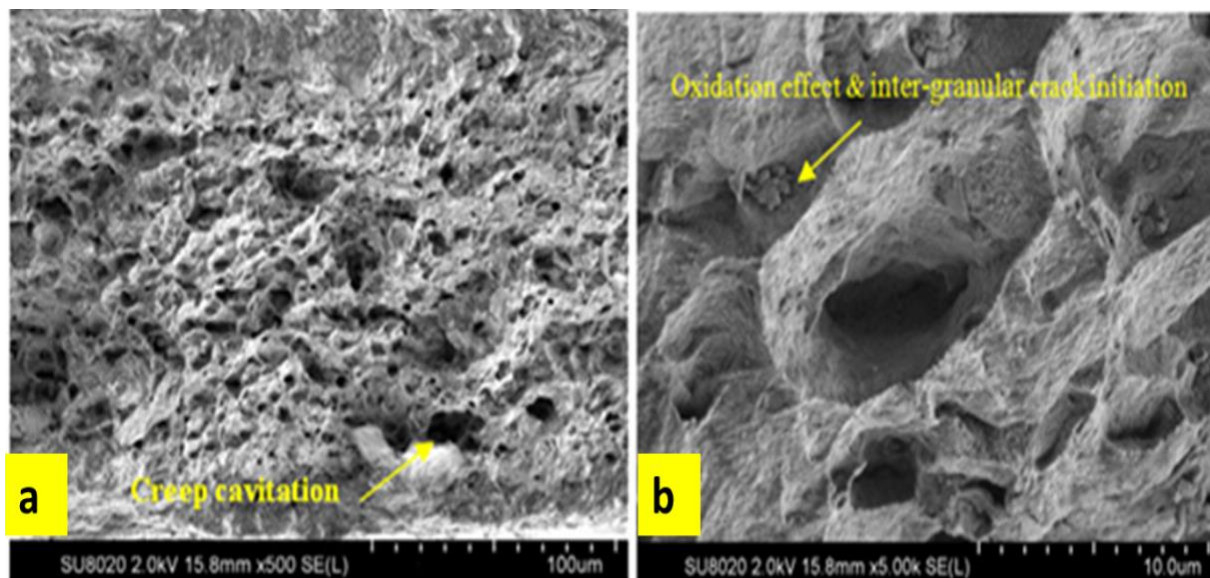
Fig. 5   Surface morphology of 2.25Cr–1Mo foil at 1027 K and 150 MPa in a different scale.

5.3. Hyperbolic Sine Model for 2.25Cr–1Mo Alloy

Figure 6 shows the variation of creep strain with creep exposure of the 2.25Cr–1Mo steel at 973, 1023, 1073 K for stresses 110, 130 and 150 MPa. From these curves, it is obvious that for temperatures between 973 to 1073 K, the primary creep regions are pretty small and there are wide regions of steady state creep for each specimen. In order to fit this experimental creep data, a phenomenological creep model such as the following form can be used:

$$\dot{\varepsilon}_{cr} = f(\sigma, T) \tag{8}$$

Hence the hyperbolic sine model can be used to fit the experimental creep data. This model is just included the steady state creep step and the time hardening or strain hardening terms, which are used to model the primary creep region, are not considered. This is a rational assumption as respects the contribution of the primary creep is inconsequential and can be ignored.

The ability of hyperbolic sine model to describe the

creep behavior of 2.25Cr–1Mo alloy at elevated temperatures was investigated. Towards this end, the hyperbolic sine model was used to fit the observed experimental creep data obtained from section 2. This producer was implemented based on the methodology described in section 3. Therefore, in this section the results of uniaxial creep tests are used to implement the constitutive analysis based on the hyperbolic sine model. In order to carry out the constitutive analysis, the steady state creep data were intercepted from the results shown in "Figs. 4 and 6". Then the methodology described in section 3 was followed.

The relationships between the logarithmic stress ln [sinh $(\alpha\sigma)$] and the logarithmic strain rate, ln $\dot{\varepsilon}_{cr}$, at different temperature are shown in "Fig. 7". In fact, this figure shows different parallel temperature lines for calculation of average stress exponent. The value of the stress multiplier α is equal to 0.0078 MPa^{-1}. This value of α gives the most acceptable fit of the experimental data for all test temperatures. The average stress exponent value, n, is 5.3 with a maximum deviation of 2.1% for the 973, 1023 and 1073 K.
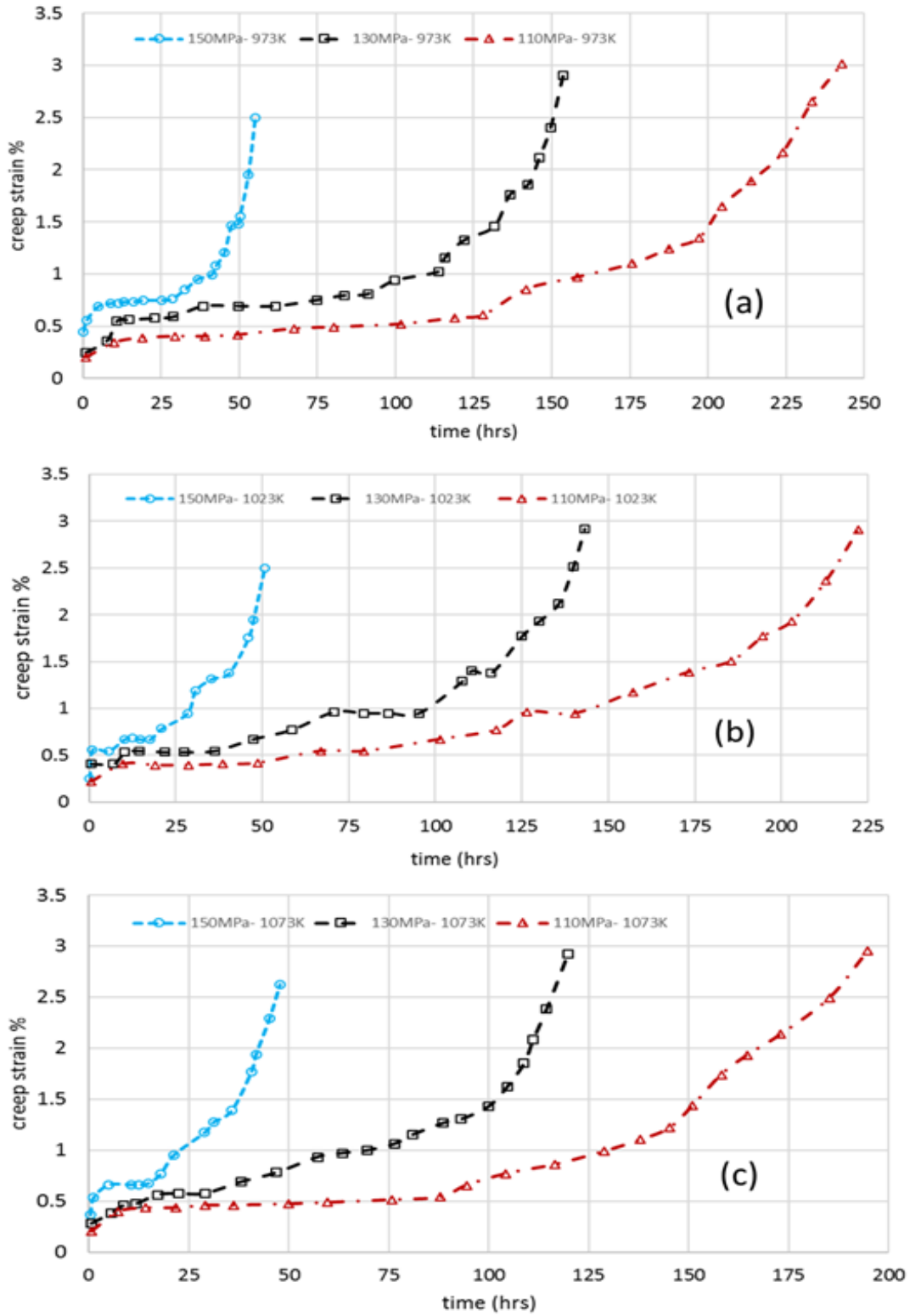
Fig. 6   Creep strain versus time for 2.25Cr–1Mo steel at: (a): 110, (b):130 and (c):150 MPa for different temperatures.
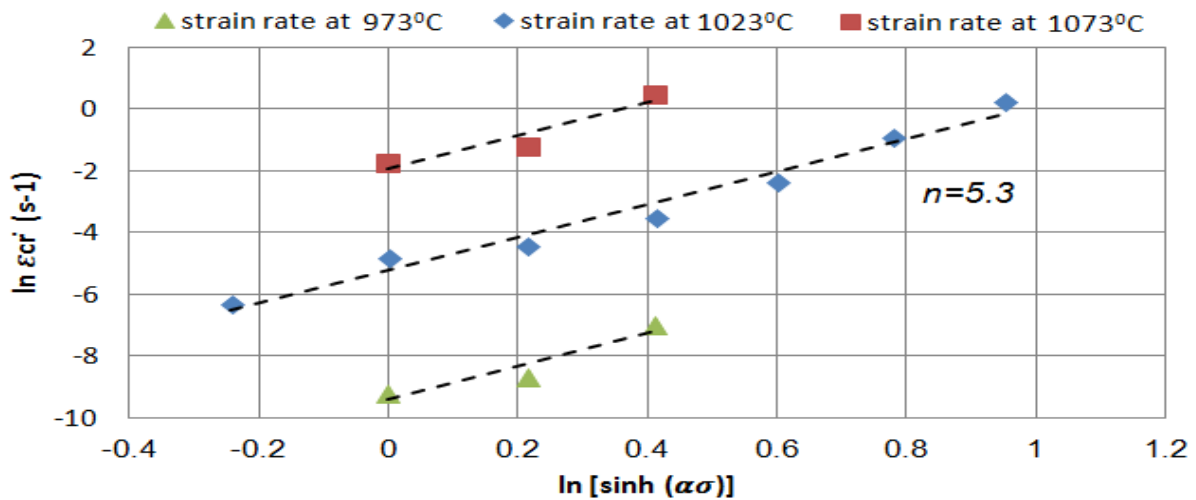
Fig. 7   Variation of ln $\dot{\varepsilon}_{cr}$ against ln [sinh ($\alpha\sigma$)] of the specimens for different temperature.

The variation in ln $\dot{\varepsilon}_{cr}$ as a function of the reciprocal of temperature is given in "Fig. 8". The activation energy, Q, of specimens estimated using "Eq. 3" was 409 kJ mol^{-1}. The logarithmic values of Z can be calculated from "Eq. 4". Figure 8 shows the variation of ln Z against ln [sinh ($\alpha\sigma$)] considering Q and n obtained from the previous steps of constitutive analysis. Based on "Fig. 9", a linear relationship can be observed between ln Z and ln [sinh ($\alpha\sigma$)] that can be used to calculate the material constant A, from the standard deviation of different temperature levels. According to this methodology, the value of A was estimated 8.23e $^{-5}$ S^{-1} for 1023 K. It can be said that the slope of different fitted curves for different elevated temperatures are close with each other and the model parameters are characterized with good accuracy. "Table 2" shows the creep hyperbolic sine parameters extracted from the constitutive analysis presented in this section for the stress range studied in the current paper.
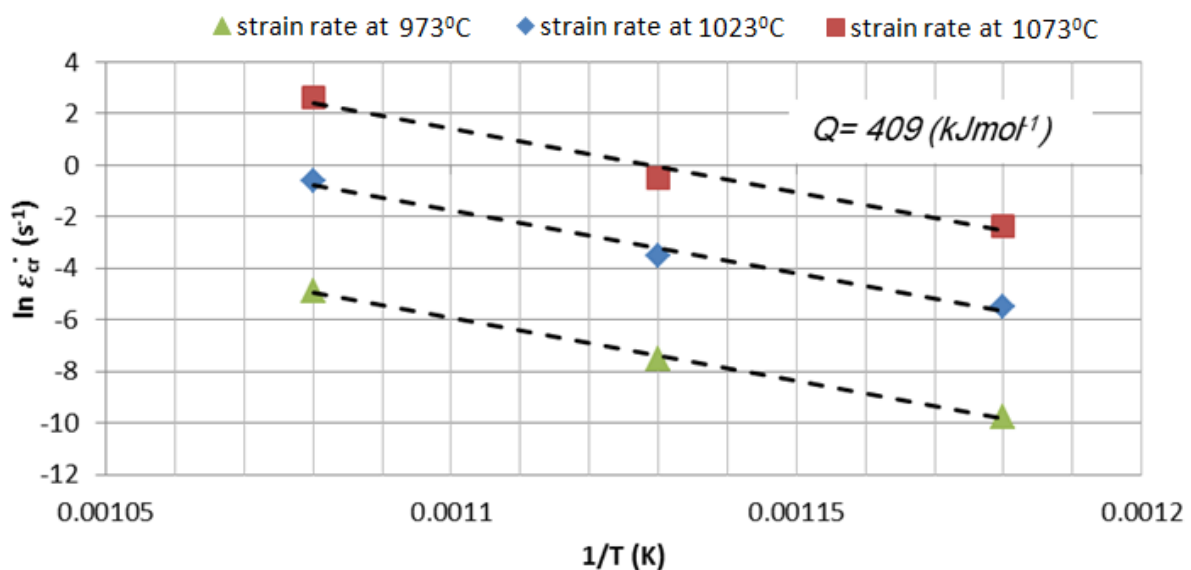
Fig. 8   Variation in ln $\dot{\varepsilon}_{cr}$ as a function of $1/T$ for the specimens at various temperatures and strain rates.
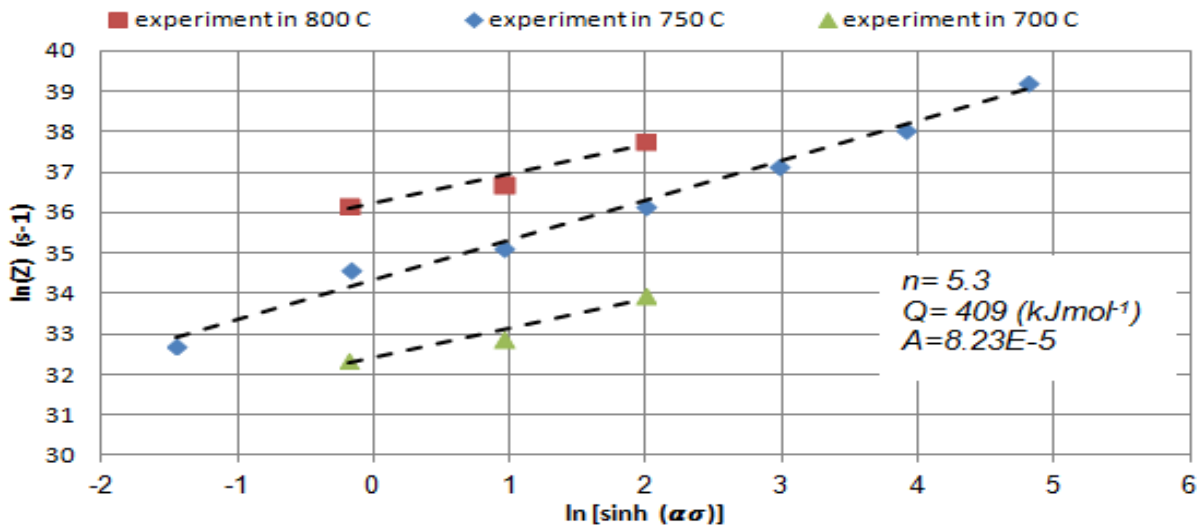
Fig. 9   Variation of the ln Z vs. ln [sinh ($\alpha\sigma$)] in different stresses and temperatures.

Table 2 Creep hyperbolic sine parameters at 1023 K

Creep hyperbolic sine parameters	A(s^{-1})	α (MPa^{-1})	Q (kJmol^{-1})	n
Value	8.23e^{-5}	0.0078	409	5.3

0.37% CEEQ at 90 MPa within 378 hrs   0.69% CEEQ at 110 MPa within 101 hrs   0.95% CEEQ at 130 MPa within 71 hrs   0.98% CEEQ at 150 MPa within 29 hrs   1.18% CEEQ at 170 MPa within 14 hrs   3.08% CEEQ at 190 MPa within 9.5 hrs   3.17% CEEQ at 210 MPa within 3.7 hrs

creep strain contour at 210 MPa

Fractured sample at 210 MPa
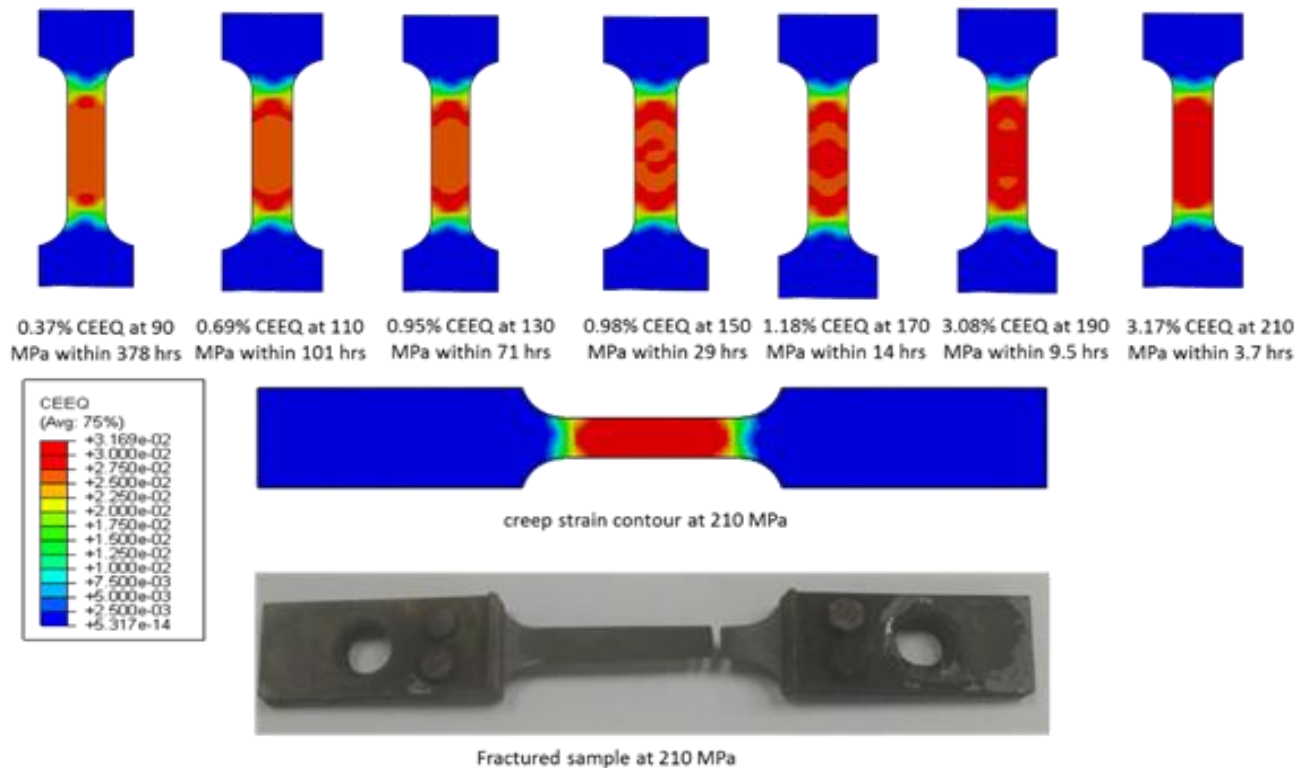
Fig. 10   CEEQ for different applied stresses at 1023K using the hyperbolic sine model in the FE analysis.
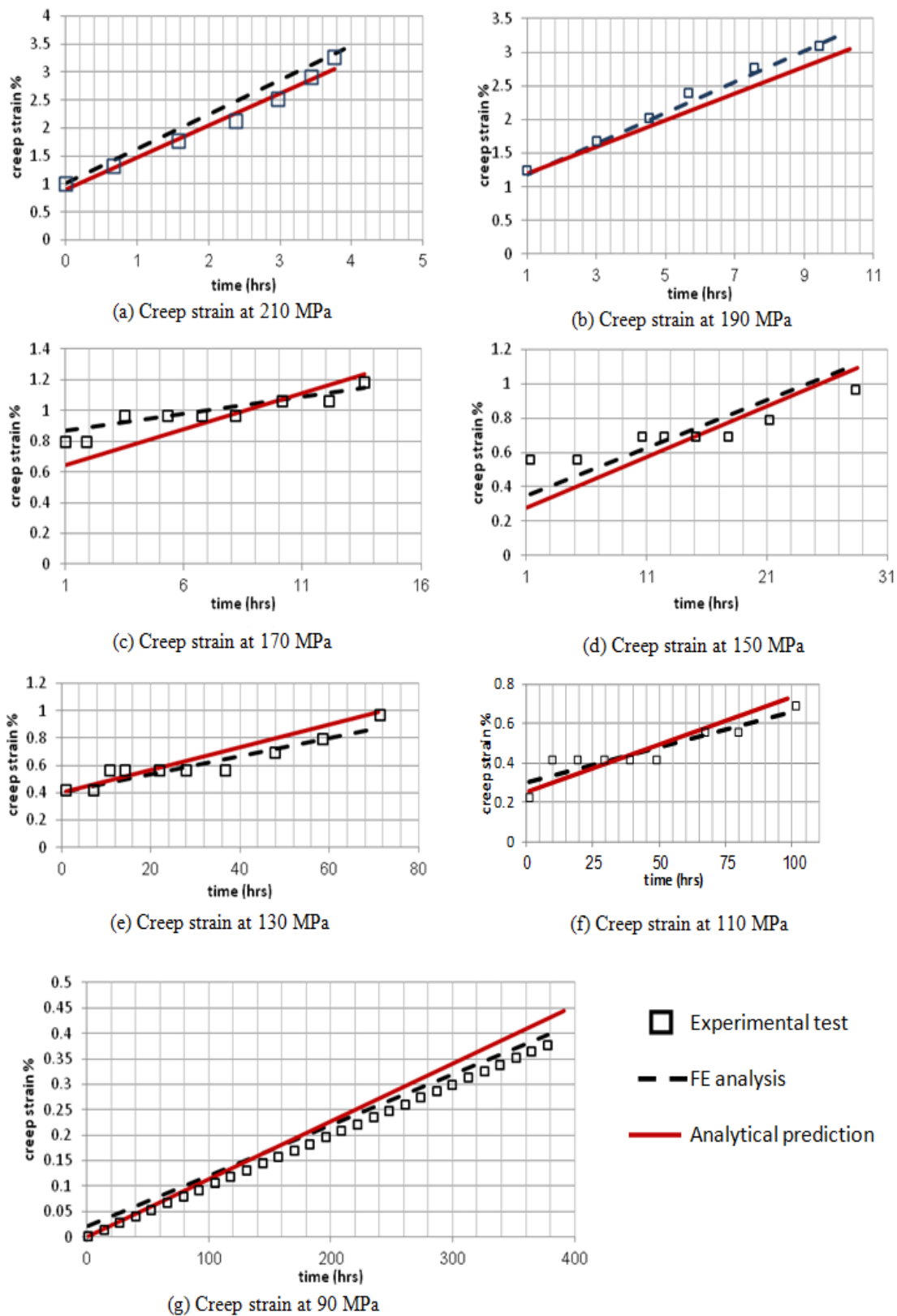
Fig. 11   Creep strain (%) during the time from the experiment, FE analysis and analytical prediction in different applied stresses at 1023K.

5.4. Possibility of using Hyperbolic Sine Model in FE Analysis

A steady state FE analysis, based on the procedure explained in section 4, was conducted to investigate the possibility of using the hyperbolic sine model in the FE simulation of creep behavior of 2.25Cr–1Mo. Figure 10 shows the equivalent creep strain contours (CEEQ) for different levels of applied stress. In addition, an experimental fractured specimen and its respective CEEQ from FE analysis at 210 MP are displayed in this figure as a sample. From "Fig. 10", it is obvious that for all specimens, the equivalent creep strain value at the center area of the specimen is large, while at the up and down areas of the specimen, it is small. This is due to the initiation of necking in the center area of the specimen and thus the strain localizes in this region.

Figure 11 shows a comparison of the creep life as predicted by the three methods i.e. experimental, analytical and FE simulation for the given creep test conditions e.g. at 1027 K and in the stress range 90 to 210 MPa. From the comparison of the standard deviation in the three approaches, it is observed that the steady state creep life of the both analytical and FE methods based on the hyperbolic sine model provide a good match with the experimental results. Hence, it can be expressed that the extracted data might be applicable to the entire testing temperatures.

The steady state creep results obtained from the FE model are plotted with the experimental results in logarithmic scale and displayed in "Fig. 12". As shown in this figure, the FE approach based on the hyperbolic sine law is fairly effective at predicting the steady state creep behavior for the temperature 1023 K for each of the stress levels.
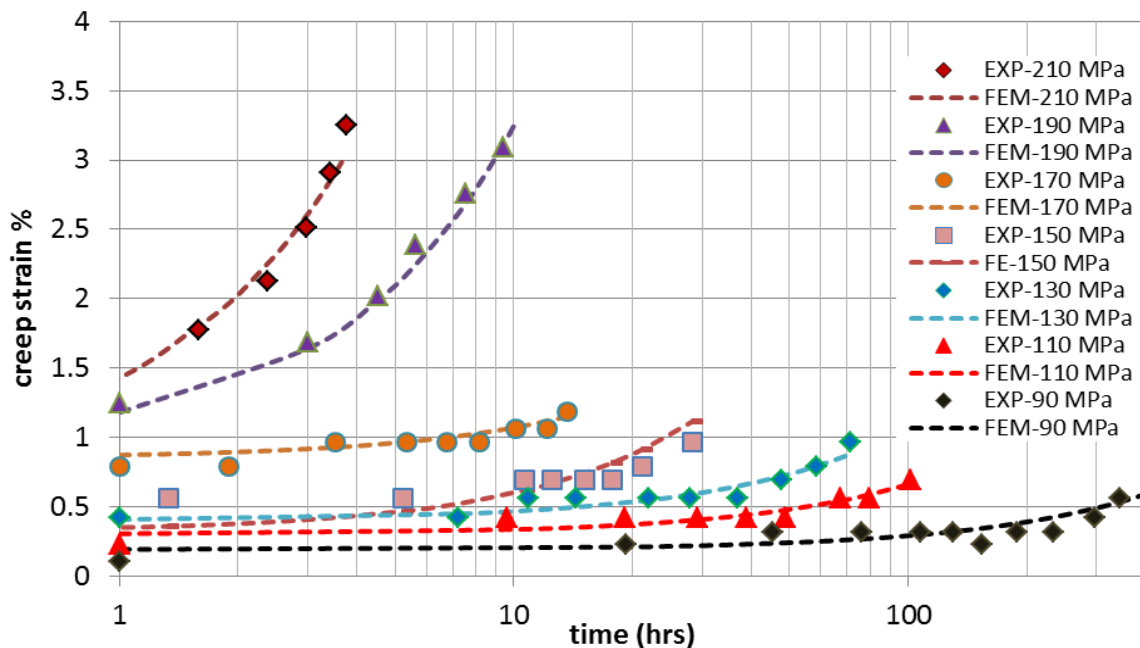
Fig. 12   Experimental creep curves and ABAQUS fit for 1023 K in the stress range of 90 to 210 MPa.

6   CONCLUSION

In this paper, steady state creep behaviour of 2.25Cr-1Mo steel alloy at elevated temperature was investigated experimentally and numerically. A creep model based on the hyperbolic sine law was presented that can be used for modelling steady state creep in 2.25Cr-1Mo steel alloy foil. The model parameters were fitted to experimental creep data for 2.25Cr-1Mo steel alloy and the best fit parameters were obtained for different temperatures and stress levels. The model was able to accurately predict steady state creep strain in the stress range of 90 to 210 MPa at temperature 1023 K. A FE model based on the parameters extracted from the hyperbolic equation was developed for predicting the steady state creep life of specimen. Results achieved from this FE model indicated a good agreement with experimental data obtained from the present work. Moreover, the Creep Failure Mechanism was analyzed by FESEM in which extensive carbides precipitation, particularly in the grain, was observed. Also, it was demonstrated that at the elevated temperature, chromium atoms diffuse to the grain boundary and form carbide precipitates so that, it leads to inter-granular fracture in the material.

REFERENCES

[1] Alipour. R., Nejad, A. F., Creep Behaviour Characterisation of a Ferritic Steel Alloy Based on the Modified Theta-Projection Data at an Elevated Temperature, International Journal of Materials Research, Vol. 107, No. 5, 2016, pp. 406-412, DOI.10.3139/146.111362.

[2] Huang, X. Z., Wang, D., and Yang, Y. T., Effect of Precipitation on Intergranular Corrosion Resistance of 430 Ferritic Stainless Steel, Journal of Iron and Steel Research, International, Vol. 22, No.11, 2015, pp. 1062-1068, DOI.10.1016/S1006-706X(15)30113-8.

[3] Gao, F., Yu, F. X., Liu, F. T., and Liu Z. Y., Hot Deformation Behavior and Flow Stress Prediction of Ultra Purified 17% Cr Ferritc Stainless Steel Stabilized with Nb and Ti, Journal of Iron and Steel Research, International, Vol. 22, No. 9, 2015, pp. 827-836, DOI.10.1016/S1006-706X(15)30077-7.

[4] Pardoen, T., Massart, T. J., Interface Controlled Plastic Flow Modelled by Strain Gradient Plasticity Theory, Comptes Rendus Mécanique, Vol. 340, No. 4-5, 2012, pp. 247-260, 4, DOI.10.1016/. 2012.02.008.

[5] Goyal, S., Laha, K., Creep Life Prediction of 9Cr–1Mo Steel Under Multiaxial State of Stress, Materials Science and Engineering: A, Vol. 615, No. 1, 2014, pp. 348-360, DOI.1016 /j.msea .2014.07.096.

[6] Ren, S., Mazière, M., Forest, S., Morgeneyer, T. F., and Rousselier, G., A Constitutive Model Accounting for Strain Ageing Effects on Work-Hardening, Application to a C–Mn Steel, Comptes Rendus Mécanique, Vol. 345, No.12, 2017, pp. 908-921, DOI. 10.1016/j.crme.2017.09.005

[7] Goyal, S., Laha, K., Das, C., Panneerselvi, S., and Mathew, M., Finite Element Analysis of Effect of Triaxial State of Stress on Creep Cavitation and Rupture Behaviour of 2.25 Cr–1Mo Steel, International Journal of Mechanical Sciences, Vol. 75, No. 1, 2013, pp. 233-243, DOI. 10.1016 /j.ijmecsci.2013.07.005.

[8] Goyal, S., Laha, K., Das, C., Selvi, S. P., and Mathew, M., Finite Element Analysis of Uniaxial and Multiaxial State of Stress on Creep Rupture Behaviour of 2.25 Cr–1Mo Steel, Materials Science and Engineering: A, Vol. 563, No. 1, 2013, pp. 68-77, DOI. 10.1016/j.msea.2012.11.038.

[9] Humphries, S., Yeung, W., and Callaghan, M. D., The Effect of Stress Relaxation Loading Cycles on the Creep Behaviour of 2.25 Cr–1Mo Pressure Vessel Steel, Materials Science and Engineering: A, Vol. 528, No. 3, 2011, pp. 1216-1220, DOI. 10.1016/j.msea.2010.10.014.

[10] Abedini, M., Mutalib, A. A., Raman, S. N., Alipour, R., and Akhlaghi, E., Pressure–Impulse (P–I) Diagrams for Reinforced Concrete (RC) Structures: A Review, Archives of Computational Methods in Engineering, 2018, pp. 1-35, DOI. 10.1007/s11831-018-9260-9

[11] Kumar, M. M., Joshna, K., Markendeya, R., and Rawat, M., Effect of Steamside Oxidation and Fireside Corrosion Degradation Processes on Creep Life of Service Exposed Boiler Tubes, International Journal of Pressure Vessels and Piping, Vol. 144, No. 1, 2016, pp. 45-48, DOI. 10.1016.2016.05.001.

[12] Nguyen, T. D., Sawada, K., Kushima, H., Tabuchi, M., and Kimura, K., Change of Precipitate Free Zone During Long-Term Creep in 2.25 Cr–1Mo Steel, Materials Science and Engineering: A, Vol. 591, No. 1, 2014, pp. 130-135, DOI. 10.1016/ j.msea.2013.10.101.

[13] Chen, J., Liu, H., Pan, Z., Shi, K., Zhang, H., and Li, J., Carbide E-Volution and Service Life of Simulated Post Weld Heat Treated 2.25 Cr–1Mo Steel, Materials Science and Engineering: A, Vol. 622, No. 1, 2015, pp. 153-159.

[14] Chaudhuri, S., Roy, N., and Ghosh, R., Modelling High Temperature Creep of Cr☐ Mo steel, Acta Metallurgica et Materialia, Vol. 41, No. 1, 1993, pp. 273-278.

[15] Hore, S. Ghosh, R., Computer Simulation of the High Temperature Creep Behaviour of Cr–Mo Steels, Materials Science and Engineering: A, Vol. 528, No. 19-20, 2011, pp. 6095-6102.

[16] Jelwan, J., Chowdhury, M., and Pearce, G., Design for Creep: a Critical Examination of Some Methods, Engineering Failure Analysis, Vol. 27, No. 1, 2013, pp. 350-372.

[17] Wang, S. B., Chang, X. F., and Key, J., New Insight into High-Temperature Creep Deformation and Fracture of T92 Steel in Volving Precipitates, Dislocations and Nanovoids, Materials Characterization, Vol. 127, No. 1, 2017, pp. 1-11, DOI. 10.1016/j.matchar.2017.01.025.

[18] Vershinina, T., Leont'eva-Smirnova, M., Dislocation Density E-Volution in the Process of High-Temperature Treatment and Creep of EK-181 Steel, Materials Characterization, Vol. 125, No. 1, 2017, pp. 23-28, DOI.10.1016/j.matchar. 2017. 01. 018.

[19] Lasseux, D., Valdés-Parada, F. J., On the Developments of Darcy's Law to Include Inertial and Slip Effects, Comptes Rendus Mécanique, Vol. 345, No. 9, 2017, pp. 660-669, DOI.10.1016 2017.06.005.

[20] Kang, G. Z., Zhang, J., Sun, Y. F., and Kan, Q. H., Uniaxial Time-Dependent Ratcheting of SS304 Stainless Steel at High Temperatures, Journal of Iron and Steel Research, International, Vol. 14, No. 1, 2007, pp. 53-59, DOI.10.1016/S1006-706X(07)60012-0.

[21] Toulemonde, C., Masson, R., and El Gharib, J., Modeling the Effective Elastic Behavior of Composites: a Mixed Finite Element and Homogenisation Approach, Comptes Rendus Mécanique, Vol. 336, No. 3, 2008, pp. 275-282, DOI.10.1016/j.crme.2007.11.024.

[22] Khayatzadeh, S., Tanner, D. W. J., Truman, C. E., P. Flewitt, E. J., and Smith, D. J., Creep Deformation and

Stress Relaxation of a martensitic P92 steel at 650 °C, Engineering Fracture Mechanics, 2017, No. 1, DOI.10.1016 /j.engfracmech.2017.02.008

[23] Boccaccini, D. N., Frandsen, H. L., Sudireddy, B. R., Blennow, P., Persson, Å. H., Kwok, K., and et al., Creep Behaviour of Porous Metal Supports for Solid Oxide Fuel Cells, International Journal of Hydrogen Energy, Vol. 39, No.36, 2014, DOI. 10.1016/j.ijhydene.2014.07.138.

[24] Strang, A., Cawley, J., and Greenwood, G. W., Microstructural Stability of Creep Resistant Alloys for High Temperature Plant Applications, 1997.

[25] Wen, J. F., Tu, S. T., Gao, X. L., and Reddy, J. N., Simulations of Creep Crack Growth in 316 Stainless Steel Using a Novel Creep-Damage Model, Engineering Fracture Mechanics, Vol. 98, No. 1, 2013, pp. 169-184, DOI.10.1016/2012.12.014.

[26] Lin, Y. C., Xia, Y. C., Ma, X. S., Jiang, Y. Q., and Chen, M. S., High-Temperature Creep Behavior of Al–Cu–Mg Alloy, Materials Science and Engineering: A, Vol. 550, No. 1, 2012, pp. 125-130, DOI.10.1016/j.msea.2012.04.044.

[27] Lin, Y. C., Xia, Y. C., Ma, X. S., Jiang, Y. Q., and Li, L. T., Modeling the Creep Behavior of 2024-T3 Al Alloy, Computational Materials Science, Vol. 67, No. 1, 2013, pp. 243-248, DOI.org/10.1016/2012.09.007.

[28] Kariya, Y., Otsuka, M., and Plumbridge, W., The Constitutive Creep Equation for a Eutectic Sn-Ag Alloy Using the Modified Theta-Projection Concept, Journal of Electronic Materials, Vol. 32, No. 12, 2003, pp. 1398-1402, DOI.1007/s11664-003-0107-1

[29] Day, W. D., Gordon, A. P., A Modified Theta Projection Creep Model for a Nickel-Based Super-Alloy, in ASME Turbo Expo 2013: Turbine Technical Conference and Exposition, 2013, pp. V07AT26A002.

[30] Evans, M., The θ Projection Method and Small Creep Strain Interpolations in a Commercial Titanium Alloy, Journal of Materials Science, Vol. 36, No. 12, 2001, pp. 2875-2884, DOI. 10.1023/a:1017946218860.

[31] Milne, I., Ritchie, R. O., and Karihaloo, B. L., Comprehensive Structural Integrity: Cyclic Loading and Fatigue Vol. 4: Elsevier, 2003.0080441556.

[32] Norton, F. H., The Creep of Steel at High Temperatures: McGraw-Hill Book Company, Incorporated, 1929.

[33] Mustata, R., Hayhurst, D., Creep Constitutive Equations for a 0.5 Cr 0.5 Mo 0.25 V Ferritic Steel in the Temperature Range 565 C–675 C, International Journal of Pressure Vessels and Piping, Vol. 82, No. 5, 2005, pp. 363-372.

[34] Pu, E. X., Feng, H., Liu, M., Zheng, W. J., Dong, H., and Song, Z. G., Constitutive Modeling for Flow Behaviors of Superaustenitic Stainless Steel S32654 during Hot Deformation, Journal of Iron and Steel Research, International, Vol. 23, No. 2, 2016, pp. 178-184, DOI. 10.1016/S1006-706X(16)30031-0.

[35] McQueen, H., Yue, S., Ryan, N., and Fry, E., Hot Working Characteristics of Steels in Austenitic State,

Journal of Materials Processing Technology, Vol. 53, 1995, pp. 293-310. DOI. 10.1016/0924-0136(95)01987-P.

[36] Wang, S., Luo, J., Hou, L., Zhang, J., and Zhuang, L., Identification of the Threshold Stress and True Activation Energy for Characterizing the Deformation Mechanisms During Hot Working, Materials & Design, Vol. 113, No. 1, 2017, pp. 27-36. DOI. 10.1016/j.matdes.2016.10.018.

[37] Reyes-Calderón, F., Mejía, I., and Cabrera, J., Hot Deformation Activation Energy (Q HW) of Austenitic Fe–22Mn–1.5 Al–1.5 Si–0.4 C TWIP Steels Microalloyed with Nb, V, and Ti, Materials Science and Engineering: A, Vol. 562, No. 1, 2013, pp. 46-52, DOI. 10.1016/j.msea.2012.10.091.

[38] McQueen, H., Ryan, N., Constitutive Analysis in Hot Working, Materials Science and Engineering: A, Vol. 322, No. 1, 2002, pp. 43-63.

[39] Cowan, M., Khandelwal, K., Modeling of High Temperature Creep in ASTM A992 Structural Steels, Engineering Structures, Vol. 80, No. 1, 2014, pp. 426-434, DOI. 10.1016/j.engstruct.2014.09.020.

[40] Brnic, J., Canadija, M., Turkalj, G., and Lanc, D., Structural Steel ASTM A709—Behavior at Uniaxial Tests Conducted at Lowered and Elevated Temperatures, Short-Time Creep Response, and Fracture Toughness Calculation, Journal of Engineering Mechanics, Vol. 136, No. 9, 2010, pp. 1083-1089, DOI. 10.1061/(ASCE)EM.1943-7889.0000152.

[41] Fields, B., Fields, R., Elevated Temperature Deformation of Structural Steel, 1988.

[42] Kodur, V., Dwaikat, M., Effect of High Temperature Creep on the Fire Response of Restrained Steel Beams, Materials and Structures, Vol. 43, No. 10, 2010, pp. 1327-1341, DOI. 10.1617/s11527-010-9583-y.

[43] Gales, J. A., Bisby, L. A., and Stratford, T., New Parameters to Describe High-Temperature Deformation of Prestressing Steel Determined Using Digital Image Correlation, Structural Engineering International, Vol. 22, No. 4, 2012, pp. 476-486.

[44] Yang, M., Wang, Q., Song, X. L., Jia, J., and Xiang, Z. D., On the Prediction of Long Term Creep Strength of Creep Resistant Steels, International Journal of Materials Research, Vol. 107, No. 2, 2016, pp. 133-138, DOI. /10.3139/146.111322.

[45] Liao, C., Wu, H., Wu, C., Zhu, F., and Lee, S., Hot Deformation Behavior and Flow Stress Modeling of Annealed AZ61 Mg Alloys, Progress in Natural Science: Materials International, Vol. 24, No. 3, 2014, pp. 253-265.

[46] Cui, Y., Sauzay, M., Caes, C., Bonnaillie, P., Arnal, B., Cabet, C., and et al., Modeling and Experimental Study of Long Term Creep Damage in Austenitic Stainless Steels, Engineering Failure Analysis, Vol. 58, No. 1, 2015, pp. 452-464, DOI. 10.1016/j.engfailanal.2015.08.009.

[47] Zhang, W., Jing, H., Xu, L., Zhao, L., Han, Y., and Li,

C., Numerical Investigation of Creep Crack Initiation in P92 Steel Pipes with Embedded Spherical Defects Under Internal Pressure at 650° C, Engineering Fracture Mechanics, Vol. 139, 2015, pp. 40-55, DOI. 10.1016/j.engfracmech.2015.03.043.

[48] ASTM, 139, Standard Test Methods for Conducting Creep, Creep-Rupture, and Stress-Rupture Tests of Metallic Materials, American Society for Testing and Materials, Philadelphia, EUA, 2011.

[49] Zhang, C., Qiao, J. C., Pelletier, J. M., and Yao, Y., Arrhenius Activation of Zr65Cu18Ni7Al10 Bulk Metallic Glass in the Supercooled Liquid Region, Intermetallics, Vol. 86, No. 1, 2017, pp. 88-93, DOI.10.1016/j.intermet.2017.03.017.

[50] Abbasi-Bani, A., Zarei-Hanzaki, A., Pishbin, M. H., and Haghdadi, N., A Comparative Study on the Capability of Johnson–Cook and Arrhenius-Type Constitutive Equations to Describe the Flow Behavior of Mg–6Al–1Zn Alloy, Mechanics of Materials, Vol. 71, 2014, pp. 52-61, DOI.10.1016/j.mechmat.2013.12.001.

[51] Liao, C. H., Wu, H. Y., Lee, S., Zhu, F. J., Liu, H. C., and Wu, C. T., Strain-Dependent Constitutive Analysis of Extruded AZ61 Mg Alloy Under Hot Compression, Materials Science and Engineering: A, Vol. 565, No. 2, 2013, pp. 1-8, DOI. 10.1016/j.msea.2012.12.025.

[52] Wu, H. Y., Yang, J. C., Zhu, F. J., and Wu, C. T., Hot Compressive Flow Stress Modeling of Homogenized AZ61 Mg Alloy Using Strain-Dependent Constitutive Equations, Materials Science and Engineering: A, Vol. 574, 2013, pp. 17-24, DOI. 10.1016/j.msea.2013.03.005.

[53] Zener, C., Hollomon, J. H., Effect of Strain Rate Upon Plastic Flow of Steel, Journal of Applied physics, Vol. 15, No. 1, 1944, pp. 22-32, DOI. 10.1063/1.1707363.

[54] Najarian, F., Alipour, R., Shokri-Rad, M., Nejad, A. F., and Razavykia, A., Multi-Objective Optimization of Converting Process of Auxetic Foam Using Three Different Statistical Methods, Measurement, Vol. 119, No. 1, 2018, pp. 108-116, DOI. 10.1016/j.measurement.2018.01.064.

[55] Mohsenizadeh, S., Alipour, R., Ahmad, Z., and Alias, A., Influence of Auxetic Foam in Quasi-Static Axial Crushing, International Journal of Materials Research, Vol. 107, No. 10, 2016, pp. 916-924, DOI. 10.3139/146.111418.

[56] Alipour, R., Nejad, A. F., and Izman, S., The Reliability of Finite Element Analysis Results of the Low Impact Test in Predicting the Energy Absorption Performance of Thin-Walled Structures, Journal of Mechanical Science and Technology, Vol. 29, No. 5, 2015, pp. 2035-2045, DOI. 10.1007/s12206-015-0424-3.